



# M<sup>5</sup>C regulator-mediated methylation modification patterns and tumor microenvironment infiltration characterization in lung adenocarcinoma

Hui Chen<sup>1#</sup>, Xiao-Lin Ge<sup>1#</sup>, Zhao-Yue Zhang<sup>1#</sup>, Ming Liu<sup>2,3,4</sup>, Rui-Yan Wu<sup>2,3,4</sup>, Xiao-Fei Zhang<sup>2,3,4</sup>, Li-Ping Xu<sup>1</sup>, Hong-Yan Cheng<sup>5</sup>, Xin-Chen Sun<sup>1</sup>, Hong-Cheng Zhu<sup>1,2,3,4</sup>

<sup>1</sup>Department of Radiation Oncology, The First Affiliated Hospital of Nanjing Medical University, Nanjing, China; <sup>2</sup>Department of Radiation Oncology, Fudan University Shanghai Cancer Center, Shanghai, China; <sup>3</sup>Department of Oncology, Shanghai Medical College, Fudan University, Shanghai, China; <sup>4</sup>Shanghai Key Laboratory of Radiation Oncology, Shanghai, China; <sup>5</sup>Department of Synthetic Internal Medicine, The First Affiliated Hospital of Nanjing Medical University, Nanjing, China

**Contributions:** (I) Conception and design: H Chen, HC Zhu; (II) Administrative support: HC Zhu, HY Cheng, XC Sun; (III) Provision of study materials or patients: XL G, ZY Zhang; (IV) Collection and assembly of data: H Chen, ZY Zhang, M Liu, RY Wu, XF Zhang; (V) Data analysis and interpretation: XL Ge, HC Zhu, LP Xu, M Liu; (VI) Manuscript writing: All authors; (VII) Final approval of manuscript: All authors.

<sup>#</sup>These authors contributed equally to this work.

**Correspondence to:** Xin-Chen Sun. Department of Radiation Oncology, The First Affiliated Hospital of Nanjing Medical University, Nanjing, 300 Guangzhou Road, Nanjing 210029, China. Email: sunxinchen@njmu.edu.cn; Hong-Cheng Zhu. Department of Radiation Oncology, Fudan University Shanghai Cancer Center, Shanghai 200032, China. Email: zhuhc90@163.com.

**Background:** In recent years, immunotherapy has made great progress, and the regulatory role of epigenetics has been verified. However, the role of 5-methylcytosine (m<sup>5</sup>C) in the tumor microenvironment (TME) and immunotherapy response remains unclear.

**Methods:** Based on 11 m<sup>5</sup>C regulators, we evaluated the m<sup>5</sup>C modification patterns of 572 lung adenocarcinoma (LUAD) patients. The m<sup>5</sup>C score was constructed by principal component analysis (PCA) algorithms in order to quantify the m<sup>5</sup>C modification pattern of individual LUAD patients.

**Results:** Two m<sup>5</sup>C methylation modification patterns were identified according to 11 m<sup>5</sup>C regulators. The two patterns had a remarkably distinct TME immune cell infiltration characterization. Next, 226 differentially expressed genes (DEGs) related to the m<sup>5</sup>C phenotype were screened. Patients were divided into three different gene cluster subtypes based on these genes, which had different TME immune cell infiltration and prognosis characteristics. The m<sup>5</sup>C score was constructed to quantify the m<sup>5</sup>C modification pattern of individual LUAD patients. We found that the high m<sup>5</sup>C score group had a better prognosis. The role of the m<sup>5</sup>C score in predicting prognosis was also verified in the dataset GSE31210.

**Conclusions:** Our study revealed that m<sup>5</sup>C modification played a significant role in TME regulation of LUAD. Investigation of the m<sup>5</sup>C regulation mode may have some implications for tumor immunotherapy in the future.

**Keywords:** M<sup>5</sup>C; tumor microenvironment (TME); immunotherapy; lung adenocarcinoma (LUAD)

Submitted Mar 16, 2021. Accepted for publication May 21, 2021.

doi: 10.21037/tlcr-21-351

View this article at: <http://dx.doi.org/10.21037/tlcr-21-351>

## Introduction

According to the ribonucleic acid (RNA) modification database (MODOMICS), over 150 RNA modifications

have been detected, including 5-methylcytosine (m<sup>5</sup>C), N6-methyladenosine (m<sup>6</sup>A), and N1-methyladenosine (m<sup>1</sup>A) (1,2). 5-methylcytosine (m<sup>5</sup>C) is one common methylation

modification, and plays significant roles in various biological process. m<sup>5</sup>C modification is a kind of post-transcriptional modification regulated by “writers”, “erasers”, and “readers”, which are methyltransferases, demethylases, and binding proteins, respectively.

Methylation of the cytosine at the fifth carbon position (m<sup>5</sup>C) is mediated by methyltransferases consisting of NOL1/NOP2/Sun domain family, member 1-7 (NSUN1-7), DNA methyltransferase1 (DNMT1), DNMT2, DNMT3A, and DNMT3B, while the removal process is catalyzed by demethylases such as ten-eleven translocation 2 (TET2). In addition, a group of specific RNA-binding proteins can read the m<sup>5</sup>C motif, thereby mediating its function. It has been found that m<sup>5</sup>C modification in messenger RNA (mRNA) is primarily enriched in the non-translated region (3'UTR and 5'UTR), guanine-cytosine (GC)-rich regions, and near the argonaute (AGO) protein binding site, which has a conserved sequence of AU(m<sup>5</sup>C)GANGU (3-6).

Immunotherapy has been an effective treatment against cancer, and is represented by immunological checkpoint blockades (ICBs). However, the overall response rates are still unsatisfying, especially for cancers with low mutational burdens (7). In recent years, with the development of immunotherapy, the therapeutic options for cancer treatment have undergone significant changes (8-11). Among the various immunotherapies, ICBs work by blocking the interaction between immunosuppressive receptors (immune checkpoints) expressed on the surface of immunocytes and their ligands. ICBs include a series of monoclonal antibody-based therapies. Cytotoxic T-lymphocyte-associated protein 4 (CTLA-4), programmed death 1 (PD-1) and programmed death-ligand 1 (PD-L1) are the main targets of immunotherapy (12,13). ICB has attracted widespread attention due to its persistence in reaction and its impact on the overall survival of patients. However, the challenge for clinicians is to determine who will respond to immunotherapy. The number of patients who actually benefit from immunotherapy remains small (14-16).

The complexity and strong interrelationship of the tumor microenvironment (TME), which comprises immune cells (such as macrophages, mast cells, polymorphonuclear cells, dendritic cells, natural killer (NK) cells, as well as T and B lymphocytes) and non-immune cells (including endothelial cells and stromal cells), play a key role in its development and progression (17,18). The immune cell components of the tumor are the basis for determining the fate of the tumor, as well as its invasion and metastasis. Interacting with other TME components either directly or indirectly can

lead to a variety of biological behavioral changes in tumor cells, including proliferation and angiogenesis, apoptosis, hypoxia, and immune tolerance (19). An increasing number of studies have shown that the TME has a crucial impact on tumor progression, immunotherapy response, and immune escape (20,21). Recently, one research has also showed that under a scenario of balanced autophagy in the tumor microenvironment, the infiltrating immune cells control cytokine production and secretion (22). Sacco *et al.* indicated that tumor-infiltrating immune cells could affect the tumor immunosurveillance by regulating the iron metabolism (23). Therefore, the characteristics of tumor immune infiltration can provide new strategies for the prediction of immunotherapeutic effect, the improvement of immunotherapeutic response rate, and the development of novel immunotherapeutic targets.

Recently, several studies have shown a strong association between m<sup>5</sup>C modification and TME infiltrating immune cells. Schoeler *et al.* reported that TET enzymes control antibody production and shape the mutational landscape in germinal center B cells. They found that TET2 and TET3 guide the transition of germinal center B cells to antibody-secreting plasma cells (24). Also, Li *et al.* revealed that the TET family modulates the activation of dendritic cells. TET1-inhibited monocyte-derived dendritic cells were found to significantly decrease the percentage of CD45RA<sup>+</sup>FoxP3<sup>hi</sup>-activated regulatory T (Treg) cells in the allergic rhinitis group, which might be linked to immune activation (25). Yue *et al.* found that TET2/3-deficiency in Treg cells leads to T cell activation, TET2/3 double-knockout (DKO) Treg cells exhibited a dysregulated cell surface phenotype, and TET2/3 DKO CD4<sup>+</sup> T cells induced disease in healthy mice (26). Moreover, some researches have focused on the intrinsic pathways of cancer cells, such as genomic variation and the disordered expression of m<sup>5</sup>C regulators. Chen *et al.* indicated that numerous oncogene RNAs with hypermethylated m<sup>5</sup>C sites were causally linked to their upregulation in urothelial carcinoma of the bladder, and demonstrated that Y-box binding protein 1 (Ybx1) is an m<sup>5</sup>C “reader” (27). Lastly, USUN5 expression has been verified to be related to shorter survival in glioblastoma and the high expression of USUN7 is correlated to the poor survival in low-grade gliomas (28,29).

However, the above studies only mentioned the role and mechanism of one or two regulatory factors of m<sup>5</sup>C in antitumor and immune processes, while the potential cross-talk between regulators remains uncharacterized in human cancers. Therefore, establishing a comprehensive

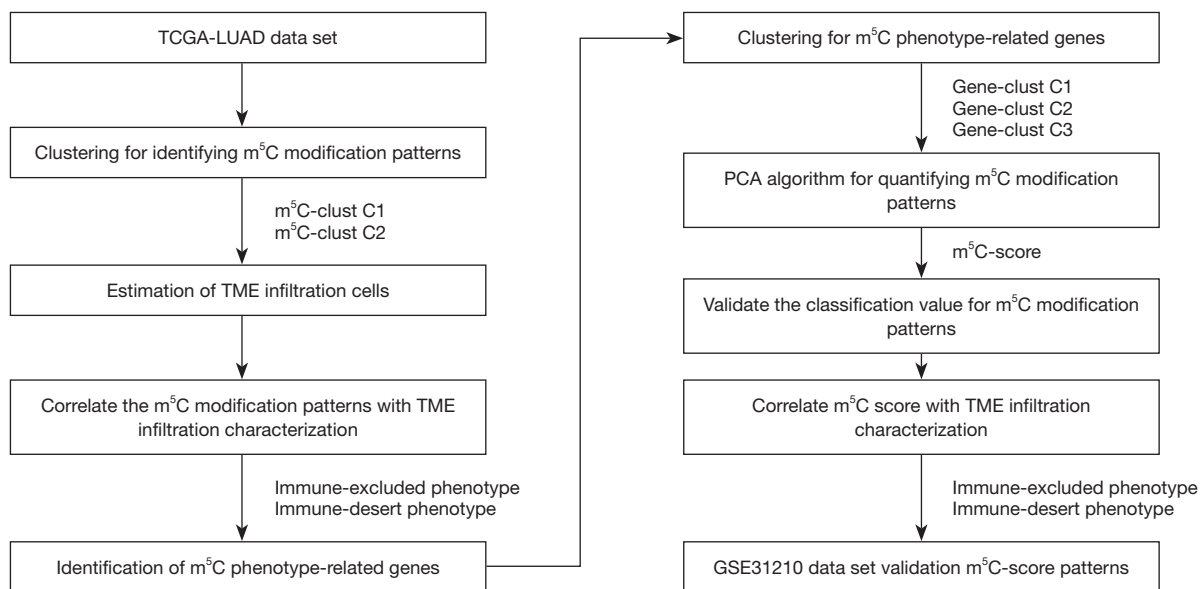


**Figure 1** Flowchart of bioinformatics analysis in our study. TCGA, The Cancer Genome Atlas; LUAD, lung adenocarcinoma; TME, tumor microenvironment.

understanding of the TME cell infiltration characterization mediated by m<sup>5</sup>C regulators will offer insight into TME immune regulation. In this study, we analyzed the gene mutation of The Cancer Genome Atlas (TCGA) lung adenocarcinoma (LUAD), the mRNA expression data, and the clinical information of patients. We also investigated the mechanisms through which m<sup>5</sup>C affected the prognosis of patients during the occurrence of LUAD, and further verified the results in an external dataset (GSE31210). We present the following article in accordance with the MDAR reporting checklist (available at <http://dx.doi.org/10.21037/tlcr-21-351>).

## Methods

### Dataset source and preprocessing

We conducted a systematic search of TCGA and the Gene-Expression Omnibus (GEO) databases for LUAD. Standardized matrix files of each cohort were downloaded for further analysis. The study was conducted in accordance with the Declaration of Helsinki (as revised in 2013). The procedure of data preprocessing lists was as follows: (I) we downloaded data of TCGA LUAD single nucleotide variation (SNV) (MuTect2 Annotation), which included 570 samples; (II) we downloaded data of TCGA LUAD copy number variation (CNV), which included 544 samples. We re-annotated the CNV of 13 genes using Bedtools

software using hg38 as a reference (30); (III) we downloaded data of TCGA LUAD FPKM (Fragments Per Kilobase Million), which included 572 samples (513 tumor samples and 59 normal samples) and 513 follow-up data; and (IV) we downloaded 246 samples of the expression profile and follow-up data of GSE31210 from National Coalition Building Institute (NCBI) GEO, which included 226 tumor samples and 20 normal samples. The study roadmap is shown in *Figure 1*.

### Unsupervised clustering for 11 m<sup>5</sup>C regulators

We extracted 11 regulators related to m<sup>5</sup>C that had expression in TCGA datasets for LUAD analysis using the prCOMP function in R language (13 genes related to m<sup>5</sup>C modification were detected, but only 11 had expression). These 13 regulators comprised 11 writers (*NSUN2*, *NSUN3*, *NSUN4*, *NSUN5*, *NSUN6*, *NSUN7*, *DNMT1*, *DNMT2*, *DNMT3B*, *NSUN1*, *DNMT3A*), one eraser (*TET2*), and one reader (Aly/REF export factor, *ALYREF*). In order to identify different m<sup>5</sup>C modification patterns and classify patients for further study, unsupervised clustering analysis was applied. The 11 m<sup>5</sup>C regulators were clustered with LUAD tumor samples by non-negative matrix factorization (NMF). The NMF method selected the standard “Brunet” and carried out 100 iterations. The number of clusters was set from 2 to 10, and we determined

the average contour width of the common member matrix using the R package “NMF”, setting the minimum members of each subclass to 10. We selected the optimal clustering number as 2 based on the cophenetic, dispersion, and silhouette.

### ***Gene set variation analysis (GSVA) and functional annotation***

In order to explore the biological behavior between these different m<sup>5</sup>C modification patterns, GSVA enrichment analysis was carried out using the R language GSVA package (31), and the “c2.cp.kegg.v7.0.symbols.gmt” gene set was used as the background. GSVA, in a non-parametric and unsupervised method, is commonly employed for estimating the variations in pathway and biological process activity in the samples of an expression dataset. Differential pathways were screened by  $|t| > 6$  using the R package limma.

### ***Estimation of TME cell infiltration***

The cell type identification by estimating relative subsets of RNA transcripts (CIBERSORT) method was used to analyze the composition and relative abundance of m<sup>5</sup>C-modified immune cells of the two patterns. Since T cells. CD4.memory.activated was 0 in all samples, we removed the cells and calculated the correlation and significance of 11 m<sup>5</sup>C-related genes and TME infiltration types through the rcorr function of the R language Hmisc package. We also used the ESTIMATE algorithm to quantify the immune, matrix, and ESTIMATE scores between groups of high and low expression regulators.

### ***Identification of differentially expressed genes (DEGs) between m<sup>5</sup>C distinct phenotypes***

Previously, two m<sup>5</sup>C modification patterns were classified by clustering m<sup>5</sup>C-related genes. In the next step, we carried out principal component analysis (PCA) of these two subtypes, and the two patterns were separated from each other. Using the R package limma package for difference analysis, 226 differential genes were screened by  $|\log_2\text{fold change}| > 1$ , false discovery rate (FDR)  $< 0.05$ . The patients were divided into different gene clusters by unsupervised clustering of 226 m<sup>5</sup>C phenotype-related genes (the distance between samples was calculated by complete and Euclidean).

### ***Generation of the m<sup>5</sup>C gene signature***

Due to the heterogeneity and complexity of m<sup>5</sup>C modification, we constructed a scoring system to quantify the m<sup>5</sup>C modification pattern of individual LUAD patients based on these phenotypic genes, which was called the m<sup>5</sup>C score. We then performed a prognostic analysis on each gene in the signature using a univariate Cox regression model. We screened 124 genes related to prognosis with  $P < 0.05$  from 226 DEGs, and subsequently analyzed the 124 genes by PCA, scored PC1 and PC2, and calculated the m<sup>5</sup>C score of each sample. The formula was as follows:

$$m^5C \text{ score} = \sum (PC1i + PC2i)$$

where  $i$  is the expression of 125 m<sup>5</sup>C phenotype-related genes.

### ***Statistical analysis***

Spearman and distance correlation analyses were utilized to compute correlation coefficients between the expression of m<sup>5</sup>C regulators and TME infiltrating immune cells. To analyze difference between two groups, the Wilcoxon test was used, and in cases of three or more groups, difference comparisons were conducted using Kruskal-Wallis tests and one-way ANOVA (analysis of variance). For verification of the external dataset GSE31210, m<sup>5</sup>C score model samples were divided into high and low score subgroups according to the median. Using the survminer R package, survival curves were generated using log-rank tests and the Kaplan-Meier (KM) method. Statistical significance was set at  $P < 0.05$ , and all statistical P values were two-sided. All data was processed using R 3.6.1 software.

## **Results**

### ***Genetic variation of m<sup>5</sup>C regulators in LUAD***

Thirteen m<sup>5</sup>C regulators were identified in this study, including 11 writers, one eraser, and one reader. We first summarized the incidence of SNV and CNV in the 13 m<sup>5</sup>C regulators in LUAD. [Figure S1](#) shows the dynamic and reversible regulation of m<sup>5</sup>C RNA methylation.

### ***SNV analysis of m<sup>5</sup>C related genes***

Of the 570 LUAD patients, gene mutations of the 13 m<sup>5</sup>C regulators appeared in 99 independent samples, with a frequency of 15.75%. The writer, DNMT3A, exhibited the highest incidence of mutation, followed by NSUN2,

TET2, and DNMT3B, while “reader” genes had fewer mutations than “writer” and “eraser” genes. *Figure 2A* displays the mutations in the top 10 genes associated with m<sup>5</sup>C, including variant classification, type, and variants per sample.

### CNV analysis of m<sup>5</sup>C related genes

In addition to SNV, CNVs are also present as genetic variations, including amplification (Segment\_Mean >0.2), diploid (-0.2 < Segment\_Mean <0.2), and deletion (Segment\_Mean <-0.2). *Table 1* shows the proportion of amplification and deletion of the 11 genes. We examined the incidence of CNV and the mRNA expression of these regulators to explore the relationship between gene variations and the expression levels of m<sup>5</sup>C regulators (*Figure 2B*), and found that CNV could be the key factor leading to the disordered expression of m<sup>5</sup>C regulators. The expression of m<sup>5</sup>C regulators in LUAD tissue was significantly higher than that in normal lung tissue (except NSUN3 and TET2) (*Figure S2*).

In total, nine CNV gene mutations had quantitative values in the gene expression profile. We observed that genes that experienced amplification showed higher expression, while those that experienced deletion exhibited lower expression. NSUN2, DNMT3B, ALYREF, and NSUN5 had a high frequency of CNV amplification, while DNMT1 and TET2 exhibited a high frequency of CNV deletion. These gene mutations may affect the transmission of the m<sup>5</sup>C signal in cells and result in cellular functional disorder. Among them, NSUN2, DNMT3b, NSUN5 and DNMT1 are writers, ALYREF is a reader, and TET2 is an eraser. Mutations of NSUN2, DNMT3b, ALYREF, NSUN5, DNMT1, and TET2 suggested that the function of m<sup>5</sup>C in tumor cells may be abnormal. The above analyses demonstrated the high heterogeneity of the genetic and expressional alteration landscape in m<sup>5</sup>C regulators between LUAD samples, indicating that the expression imbalance between m<sup>5</sup>C regulators plays a crucial role in the occurrence and progression of LUAD.

### m<sup>5</sup>C methylation modification patterns mediated by 11 regulators

#### PCA analyses of m<sup>5</sup>C-related genes

We extracted 11 m<sup>5</sup>C-related genes from TCGA and performed PCA analyses using prCOMP (there were 13 genes related to m<sup>5</sup>C modification, but only 11 genes with a quantitative expression level). The first three principal

components were shown by *pca3d* in *Figure 3A*. The 11 m<sup>5</sup>C-related samples could be completely distinguished between tumor samples and normal samples.

#### Network analyses of m<sup>5</sup>C-related genes

LUAD tumor samples from TCGA with available overall survival (OS) data and clinical information were enrolled into one meta-cohort. The prognostic values of the 11 m<sup>5</sup>C regulators were revealed via a univariate Cox regression model (*Figure 3B*). The 11 regulators were not related to the prognosis of LUAD patients, except for NSUN7, which also indicated that these 11 genes may indirectly interfere with the prognosis of LUAD patients. The m<sup>5</sup>C regulatory network described the integrated view of the mutual effect of m<sup>5</sup>C regulators, regulator connection, and their prognostic value for LUAD patients (*Figure 3C* and *Table S1*). The 11 genes were divided into four clusters. We found a correlation between expression and functional category of similar m<sup>5</sup>C regulators. ALYREF may be a key gene of m<sup>5</sup>C regulators, which affects the prognosis of LUAD through forward and reverse regulation of the other 10 genes.

### TME cell infiltration characteristics in distinct m<sup>5</sup>C modification patterns

#### Identification of m<sup>5</sup>C modified subtypes (m<sup>5</sup>C clusters)

We used the NMF R package to classify patients into two distinct modification patterns via unsupervised clustering, according to the expression quantity of 11 m<sup>5</sup>C regulators (*Figure 4A,B*). A total of 504 samples were included, including 152 samples for cluster C1 and 352 samples for cluster C2. We termed these patterns: m<sup>5</sup>C cluster C1 and C2, respectively. Furthermore, prognostic analysis for the two main m<sup>5</sup>C modification subtypes was also performed, and the results showed significant differences in OS between cluster C1 and C2 (*Figure 4C*). The m<sup>5</sup>C cluster C2 modification pattern exhibited a significant survival advantage. Then, we analyzed the expression of 11 m<sup>5</sup>C regulators in the two main m<sup>5</sup>C modification subtypes. The expression of the 7 genes among 11 regulators were significantly different between cluster C1 and C2, and all 7 genes' expression is higher in the cluster C1 (*Figure 4D*).

#### Functional enrichment of m<sup>5</sup>C modified subtypes

In order to explore the biological behavior of these different m<sup>5</sup>C modification patterns, enrichment analysis of GSEA was carried out using R language GSEA package, with the c2\_cp.kegg.v7.0.symbols.gmt gene set as a background. A

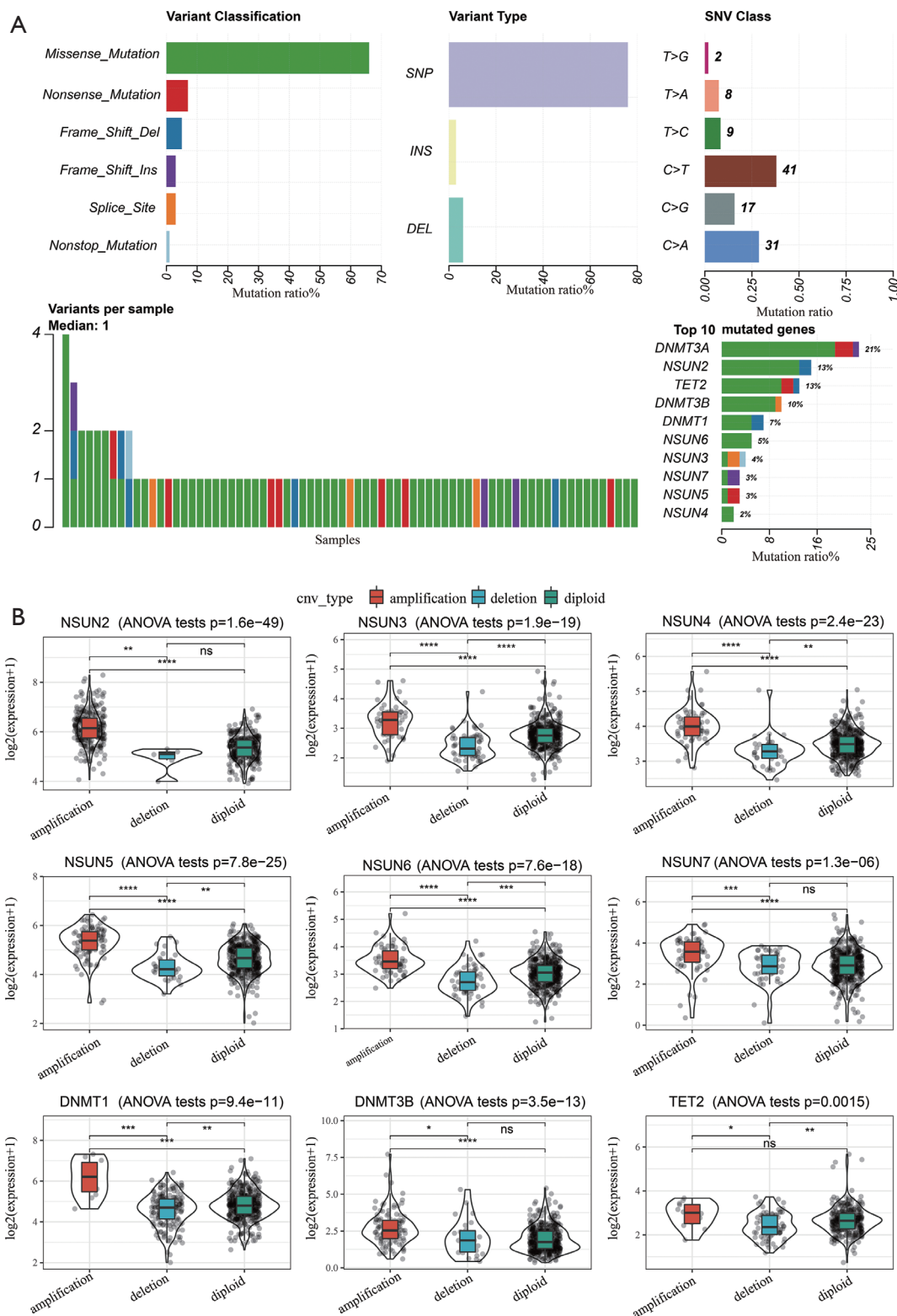


**Figure 2** Landscape of  $m^5C$  regulators in LUAD. (A) Mutations of the first 10 genes related to  $m^5C$ ; (B) the relationship between CNV and expression of nine genes related to  $m^5C$  modification. ns, no significant difference; \*,  $P < 0.05$ ; \*\*,  $P < 0.01$ ; \*\*\*,  $P < 0.001$ ; \*\*\*\*,  $P < 0.0001$ . LUAD, lung adenocarcinoma.

**Table 1** The proportion of amplification and deletion of 11 genes related to m<sup>5</sup>C modification

Role	Gene symbol	Amplification	Diploid	Deletion	CNV_sum	Amplification %	Deletion%
Writers	<i>NSUN2</i>	279	826	6	1111	25.1	0.540054
	<i>NSUN3</i>	53	985	64	1102	4.8	5.807623
	<i>NSUN4</i>	64	998	42	1104	5.8	3.804348
	<i>NSUN5</i>	102	964	32	1098	9.289617	2.91439
	<i>NSUN6</i>	67	978	57	1102	6.079855	5.172414
	<i>NSUN7</i>	62	990	48	1100	5.636364	4.363636
	<i>DNMT1</i>	12	919	174	1105	1.085973	15.74661
	<i>DNMT2</i>	72	1017	10	1099	6.55141	0.909918
	<i>DNMT3B</i>	112	967	28	1107	10.11743	2.529359
	<i>NSUN1</i>	-	-	-	-	-	-
	<i>DNMT3A</i>	-	-	-	-	-	-
Erasers	<i>TET2</i>	13	433	80	526	2.471483	15.20913
ALYREF	<i>ALYREF</i>	146	937	15	1098	13.2969	1.36612

total of 187 pathways were enriched, and 39 differential pathways were screened by  $|t| > 6$ . The m<sup>5</sup>C C1 subgroup was enriched in 14 pathways, mainly related to matrix pathways such as cell cycle and DNA (deoxyribonucleic acid) repair, while C2 was enriched in 25 pathways, mainly related to signal transduction and immune pathways (such as Fc epsilon RI signaling pathway and the mitogen-activated protein kinase (MAPK) signaling pathway) (Figure 5).

### TME analyses of m<sup>5</sup>C modified subtypes

The CIBERSORT method was used to analyze the composition of immune cells of two m<sup>5</sup>C modification patterns (32). C1 was primarily composed of naïve B cells, activated CD4 memory T cells, follicular T helper cells, resting NK cells, M0 macrophages, and M1 macrophages, while C2 was mainly composed of memory B cells, resting CD4 memory T cells, monocytes, M2 macrophages, resting dendritic cells, resting mast cells, neutrophils, and eosinophils (Figure 6A).

The correlation between m<sup>5</sup>C-related genes and TME infiltration type was calculated using the `rcorr` function of `Hmisc` package in R language. As shown in Figure 6B, the DNMT3B gene was significantly associated with 10 TME infiltrating immune cell groups, of which, six were composed of m<sup>5</sup>C modified C1 immune cells (naïve B cells, activated CD4 memory T cells, follicular T helper cells, resting NK cells, M0 macrophages and M1 macrophages).

The remaining four were composed of immune cells of the C2 subgroup (memory B cells, resting CD4 memory T cells, resting dendritic cells and resting mast cells). We used the ESTIMATE algorithm to quantify DNMT3B (Figure 6C). DNMT3B expression was inversely correlated with the immune, matrix, and ESTIMATE scores. Furthermore, we analyzed the expression of DNMT3B in 21 immune cells, and found that the low expression of DNMT3B was significantly increased in the 21 immune cells (Figure 7A).

Next, we analyzed the relationship between the expression of DNMT3B and ICB inhibitors. Abnormal expression of DNMT3B was associated with immune function disorder (Figure 7B). Subsequent analyses of pathway enrichment revealed that tumors with high DNMT3B expression exhibited enrichment in the Nod-like receptor (NLR) signaling pathway, cytosolic DNA-sensing pathway, and RIG-I-like receptor (RLR) signaling pathway (Figure 7C). Furthermore, we analyzed the OS of high and low expression groups of DNMT3B. The results showed that low DNMT3b gene expression group was associated with immunity and had a better prognosis (Figure 7D).

### Generation of m<sup>5</sup>C gene signatures and functional annotation

Using the `limma` package from R language, 226 DEGs were screened by  $|\log_2 \text{fold change}| > 1$  and  $\text{FDR} < 0.05$ ,

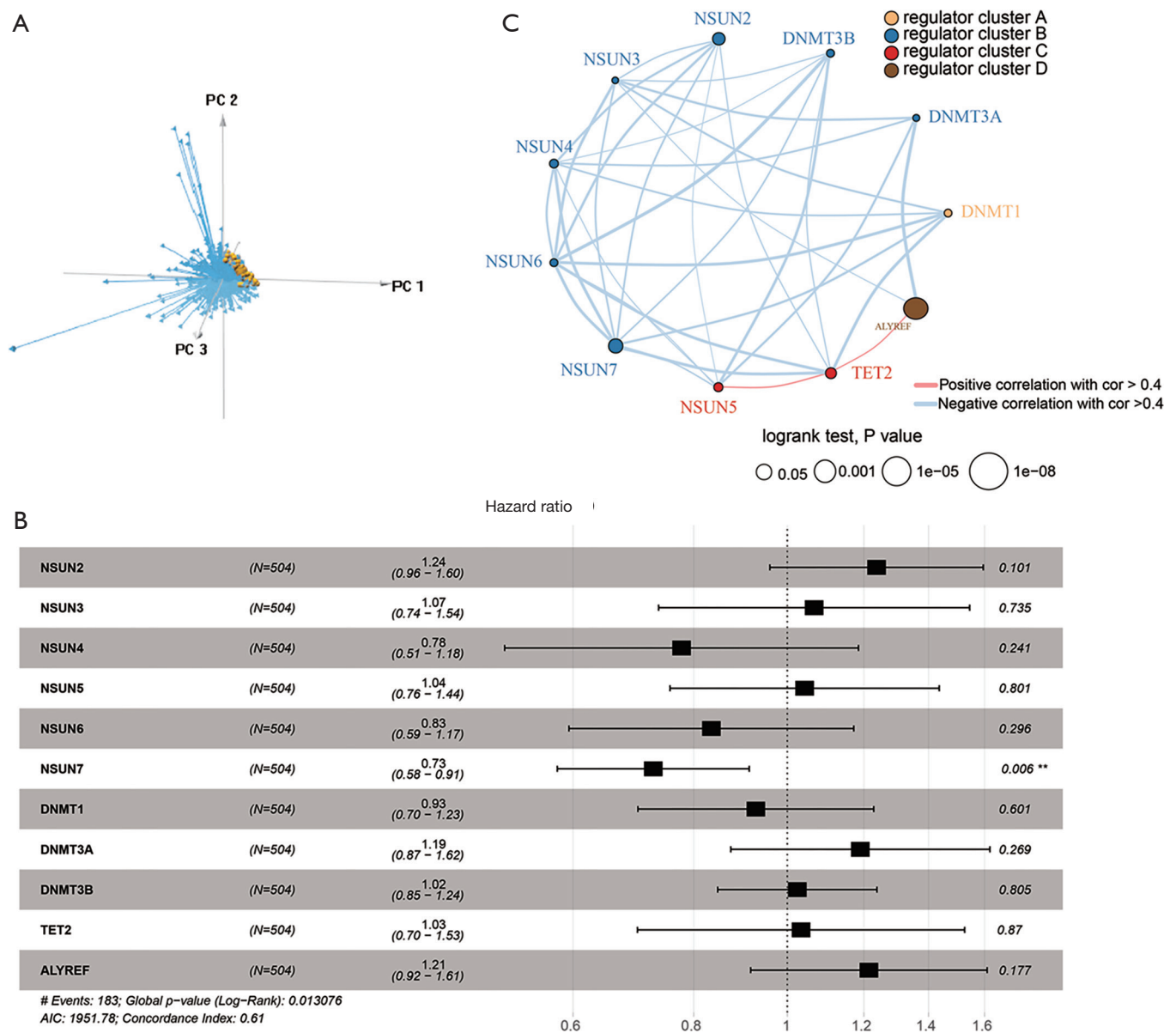


**Figure 3** M<sup>5</sup>C methylation modification patterns mediated by 11 regulators. (A) PCA for the expression of 11 m<sup>5</sup>C regulators to distinguish tumors from normal samples. Tumors were marked with blue, and normal samples were marked with yellow; (B) the prognostic analyses for 11 m<sup>5</sup>C regulators using a univariate Cox regression model; (C) the interaction between m<sup>5</sup>C regulators in LUAD. \*\*, P<0.01. PCA, principal component analysis; LUAD, lung adenocarcinoma.

all of which were related to the m<sup>5</sup>C phenotype. The patients were divided into three different gene cluster subtypes through unsupervised clustering of 226 m<sup>5</sup>C phenotype-related genes (the cluster method was complete and Euclidean was used to calculate the distance between samples). PCA analysis demonstrated that they were separated from each other (Figure 8A). These three clusters

were named m<sup>5</sup>C gene cluster C1–C3. We also observed the distribution of the 11 genes in the three m<sup>5</sup>C gene clusters (Figure 8B), and found that most samples of gene cluster C2 and C3 were included in m<sup>5</sup>C cluster C2, and most samples of gene cluster C1 coincided with m<sup>5</sup>C cluster C1. In order to further determine which biological processes these 226 genes were primarily involved in, R language WebGestaltR



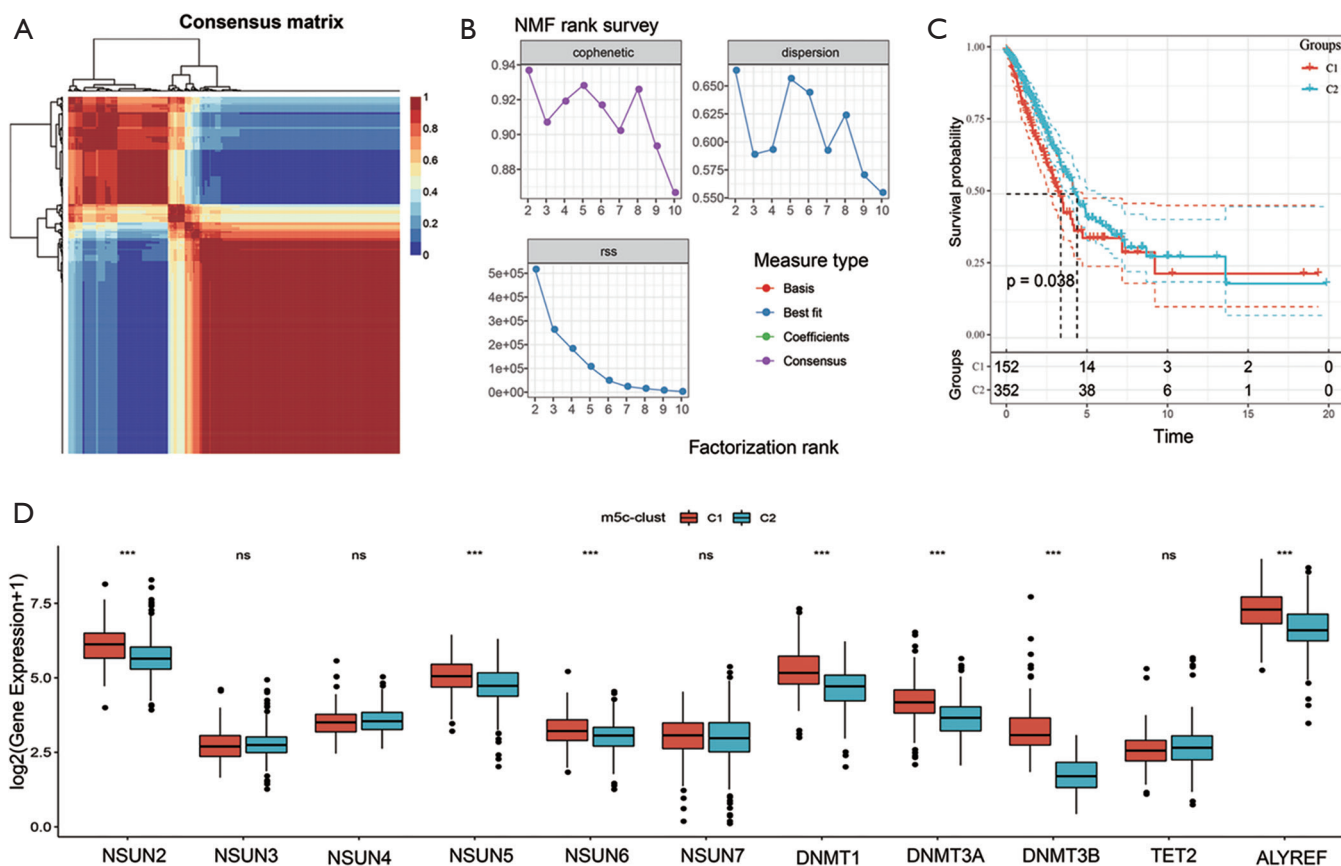


**Figure 4** Identification of m<sup>5</sup>C modified subtypes. (A) Consensus map of NMF clustering; (B) Cophenetic, RSS, and dispersion distributions with rank =2–10; (C) OS survival curves of m<sup>5</sup>C clusters C1 and C2; (D) expression of 11 genes in two m<sup>5</sup>C modification clusters. ns, no significant difference; \*\*\*, P<0.001. NMF, non-negative matrix factorization; RSS, residual sum of squares; OS, overall survival.

package was used for Kyoto Encyclopedia of Genes and Genomes (KEGG) enrichment analysis (31441146) (33). We screened a total of five pathways (by P<0.05): cell cycle, oocyte meiosis, progesterone mediated oocyte maturation, cellular sense, and the p53 signaling pathway. The 226 genes were associated with m<sup>5</sup>C modification and were significantly related to tumorigenesis (Figure 8C).

Subsequently, the distribution of 21 immune cells in the three subtypes of the m<sup>5</sup>C gene cluster was analyzed. As shown in Figure 8D, the three subtypes were statistically significant in 14 cells. Thus, it was clear that m<sup>5</sup>C modification had a critical role in TME, and the 226 genes modified by m<sup>5</sup>C also played an important role in the TME. We further analyzed the KM curve of gene clusters C1–C3, and found that these three subtypes were associated with prognosis (P<0.05, Figure 8E). Although the samples were divided into three subtypes, there were only nine cases of C3 samples. These results were consistent with the

classification of m<sup>5</sup>C modification patterns. The prognosis of C2 was superior to that of C1.

#### Establishment of the m<sup>5</sup>C score model

Due to the individual heterogeneity and complexity of m<sup>5</sup>C modification, a scoring system was constructed to quantify the m<sup>5</sup>C modification pattern of individual LUAD patients, which was called the m<sup>5</sup>C score. Firstly, we screened 124 genes related to prognosis (P<0.05) from 226 isoform differential genes. Table S2 shows the results of the univariate COX analysis of 124 genes. PCA analysis was then performed on the 124 genes, PC1 and PC2 scores were taken, and the m<sup>5</sup>C score of each sample was calculated as follows: m<sup>5</sup>C-score=ΣPC1i+PC2i. The m<sup>5</sup>C score results of the 513 samples are displayed in Table S3.

We divided the high and low score groups according to the median of the m<sup>5</sup>C score and used the alluvial diagram

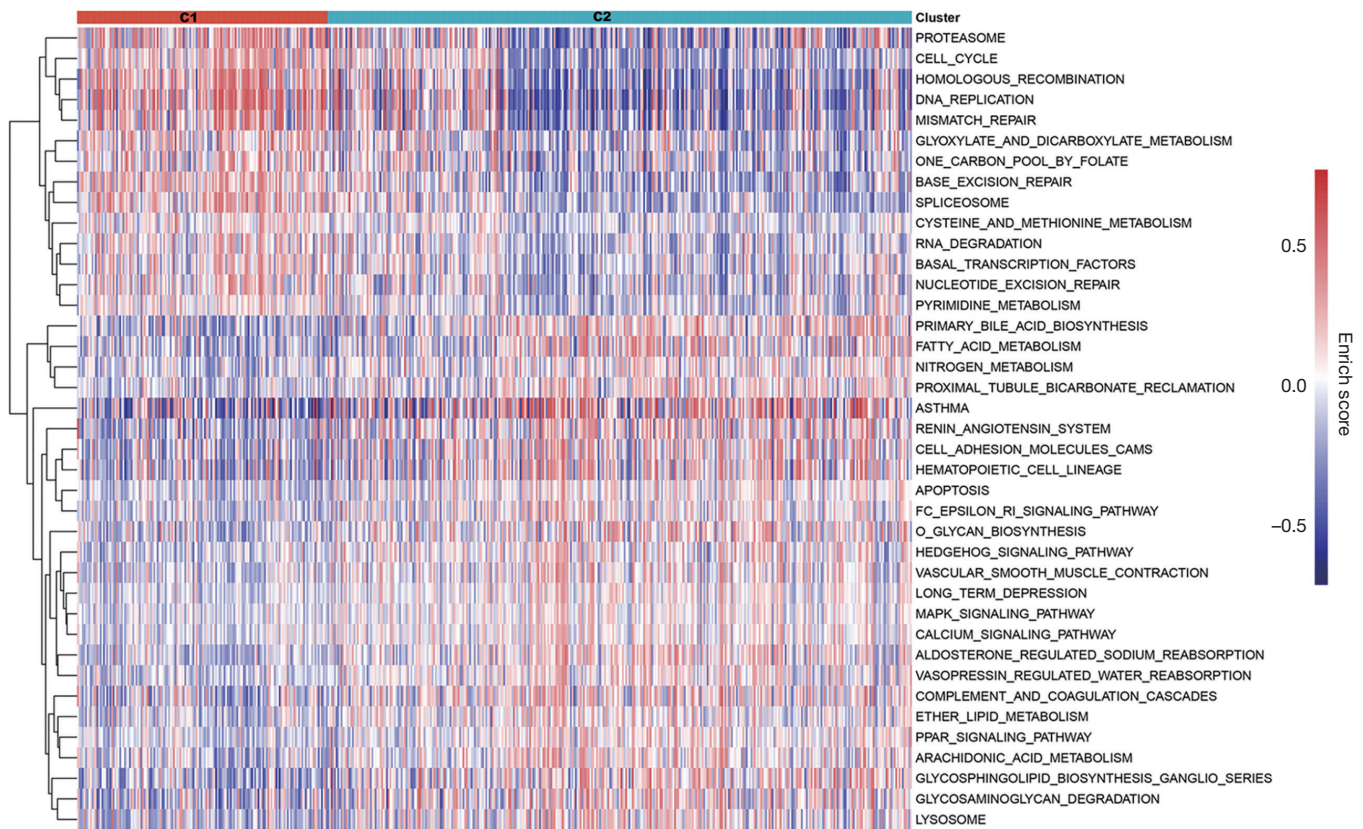


**Figure 5** Expression of 39 pathways in the GSVA analysis of two m<sup>5</sup>C modification clusters. GSVA, gene set variation analysis.

to demonstrate the changes between m<sup>5</sup>C clusters, gene clusters, and m<sup>5</sup>C scores (Figure 9A). We found that most of the samples of the m<sup>5</sup>C cluster C2 subtype with good prognosis were identical with those of the gene cluster C2 subtype, and patients with good prognosis primarily exhibited a high m<sup>5</sup>C score.

To further verify the relationship between our m<sup>5</sup>C score model and the prognosis of LUAD, we divided the high and low score groups according to the median m<sup>5</sup>C score. Survival analysis was then performed between these two groups. We observed that the high m<sup>5</sup>C score group had a better prognosis, which was consistent with the results of the previous analysis (Figure 9B).

As shown in Figure 9C, there was a significant difference in the m<sup>5</sup>C scores among the three gene cluster subtypes, with cluster C2 scoring the highest, and cluster C1 the lowest, which also verified that a high m<sup>5</sup>C score had a good prognosis. Additionally, m<sup>5</sup>C score difference was also statistically significant between the two m<sup>5</sup>C cluster subtypes (Figure 9D). The score of the C2 subtype was markedly higher than that of the C1 subtype, and the prognosis of C2

was better than that of C1, which further verified that a high m<sup>5</sup>C score had a better prognosis. Therefore, a high m<sup>5</sup>C score may predict a good prognosis for LUAD patients, while a low m<sup>5</sup>C score may predict a poor prognosis.

We also performed GSVA analysis to further explore the biological process involved in the m<sup>5</sup>C score difference. We found that the low m<sup>5</sup>C score group was mainly related to pathways of DNA repair, cell cycle, and stroma, while the high m<sup>5</sup>C score group was primarily associated with immune-related pathways and MAPK signaling pathways (Figure 9E). Furthermore, through multivariate Cox regression model analysis, we found that m<sup>5</sup>C score was an independent prognostic factor (sample with missing clinical information removed) (Figure 9F).

Moreover, we analyzed the expression of 11 m<sup>5</sup>C regulators in the high and low m<sup>5</sup>C score groups. The expression of seven regulators exhibited significant correlation with m<sup>5</sup>C score. As shown in Figure 10, in addition to TET2, a high m<sup>5</sup>C score also corresponded to low gene expression (*NSUN2*, *NSUN5*, *DNMT1*, *DNMT3A*, *DNMT3B*, and *ALYREF*).

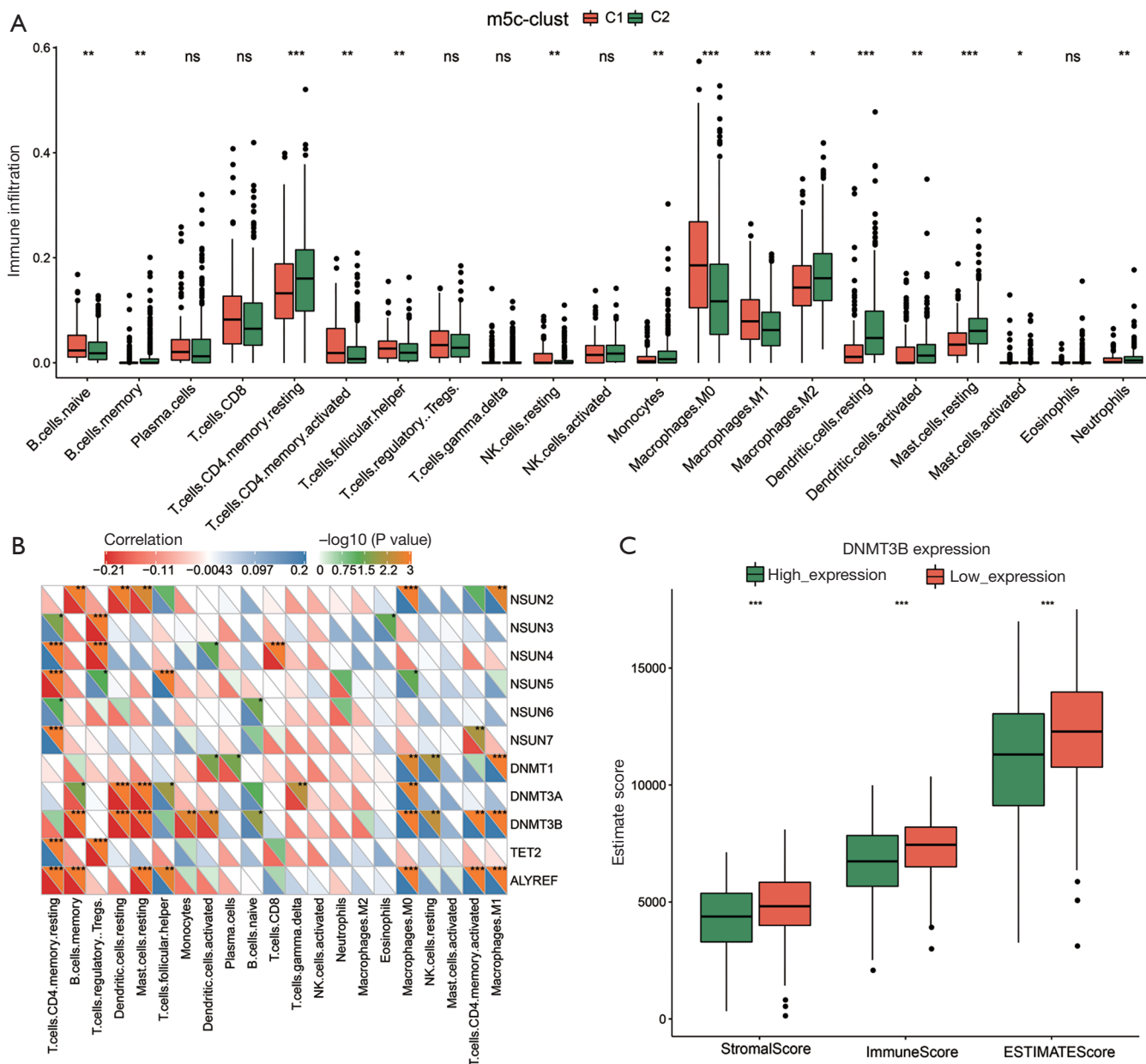


**Figure 6** TME cell infiltration characteristics and transcriptome traits in distinct m<sup>5</sup>C modification patterns. (A) The abundance of each TME infiltration cell in two m<sup>5</sup>C modification patterns; (B) the correlation between each TME infiltration cell type and each m<sup>5</sup>C regulator using Spearman analyses; (C) difference in stromal, immune, and ESTIMATE scores between high and low DNMT3B expression groups. ns, no significant difference; \*, P<0.05; \*\*, P<0.01; \*\*\*, P<0.001. TME, tumor microenvironment.

*Validation of external datasets*

**Establishment of GSE31210 dataset m<sup>5</sup>C score**

The PCA analysis results of 125 genes obtained from the previous analysis were used to establish a new m<sup>5</sup>C score model based on the GSE31210 dataset. In total, 116

genes were identified in the GSE31210 dataset, which were used to establish the m<sup>5</sup>C score model for 226 tumor samples in GSE31210. First, through PCA analysis, PC1 and PC2 of the 116 genes were calculated, and the m<sup>5</sup>C score was calculated for each sample. *Figure 11A* shows the distribution of the 11 genes in the high and low m<sup>5</sup>C



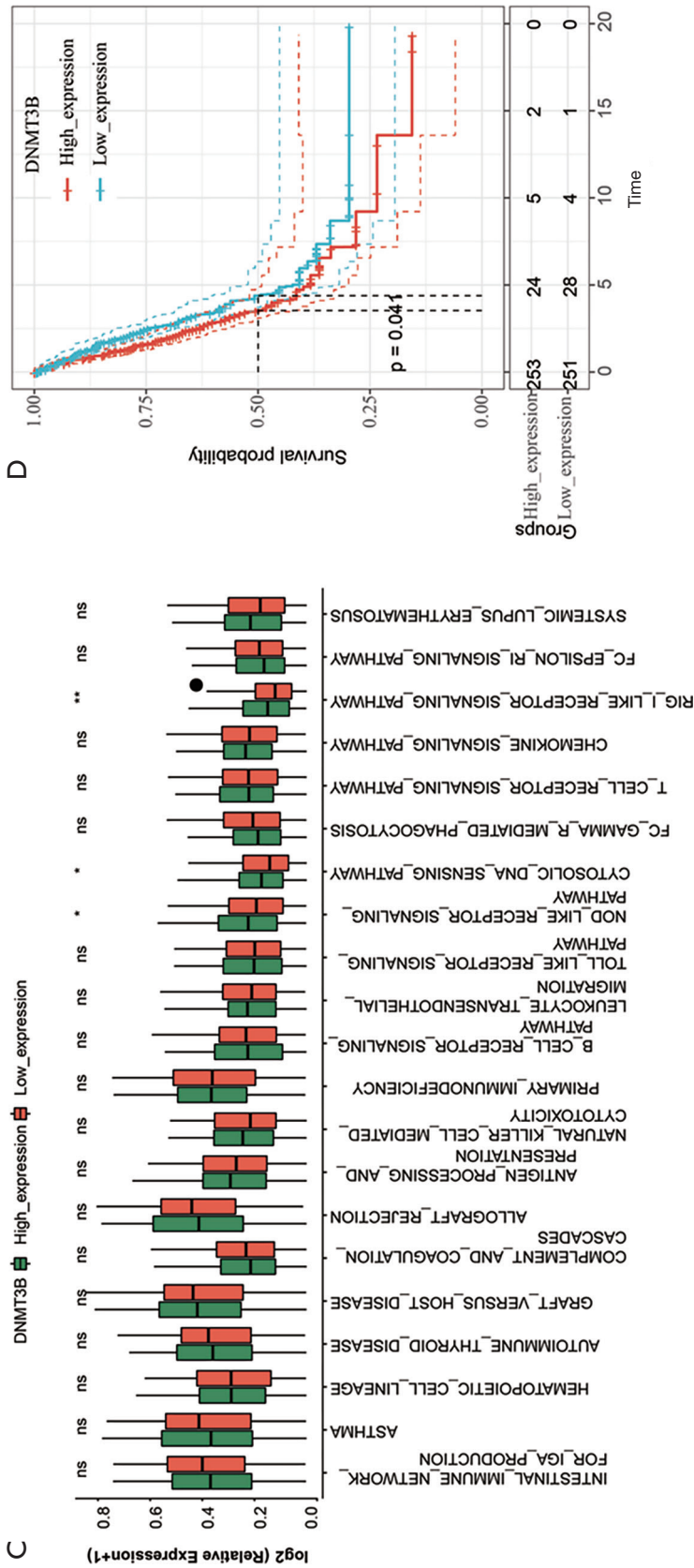


**Figure 7** The expression of DNMT3B is associated with TME. (A) Differences in the abundance of each TME infiltration cell between high and low DNMT3B expression groups; (B) differences in the expression of immune checkpoint between high and low DNMT3B expression groups; (C) differences in the immune related pathways between high and low DNMT3B expression groups; (D) survival analyses for patients with low or high DNMT3B expression. ns, no significant difference; \*, P<0.05; \*\*, P<0.01; \*\*\*, P<0.001. TME, tumor microenvironment.

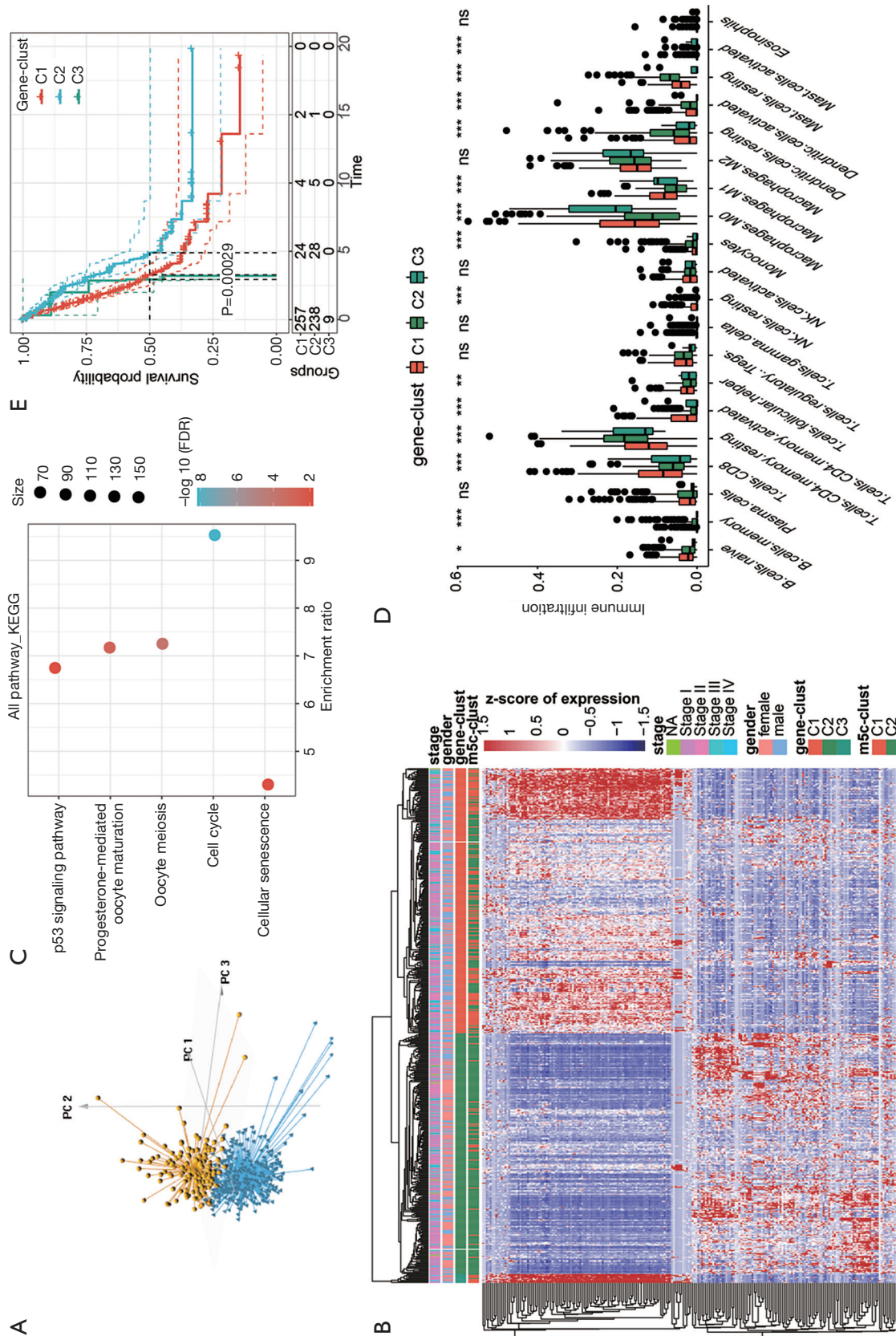


**Figure 8** Generation of m<sup>5</sup>C gene signatures and functional annotation. (A) Principal component analysis for two m<sup>5</sup>C modification patterns to distinguish m<sup>5</sup>C clusters C1 and C2; (B) unsupervised clustering of overlapping m<sup>5</sup>C phenotype-related genes was performed to classify patients into different genomic subtypes, termed m<sup>5</sup>C gene clusters C1–C3, respectively. The gene clusters, m<sup>5</sup>C clusters, gender, and stage were used as patient annotations; (C) KEGG enrichment analysis of 226 m<sup>5</sup>C phenotype-related genes; (D) the abundance of each TME infiltration cell in three m<sup>5</sup>C gene clusters; (E) survival analyses for patients of m<sup>5</sup>C gene cluster C1, C2, and C3. ns, no significant difference; \*, P<0.05; \*\*, P<0.01; \*\*\*, P<0.001. TME, tumor microenvironment.

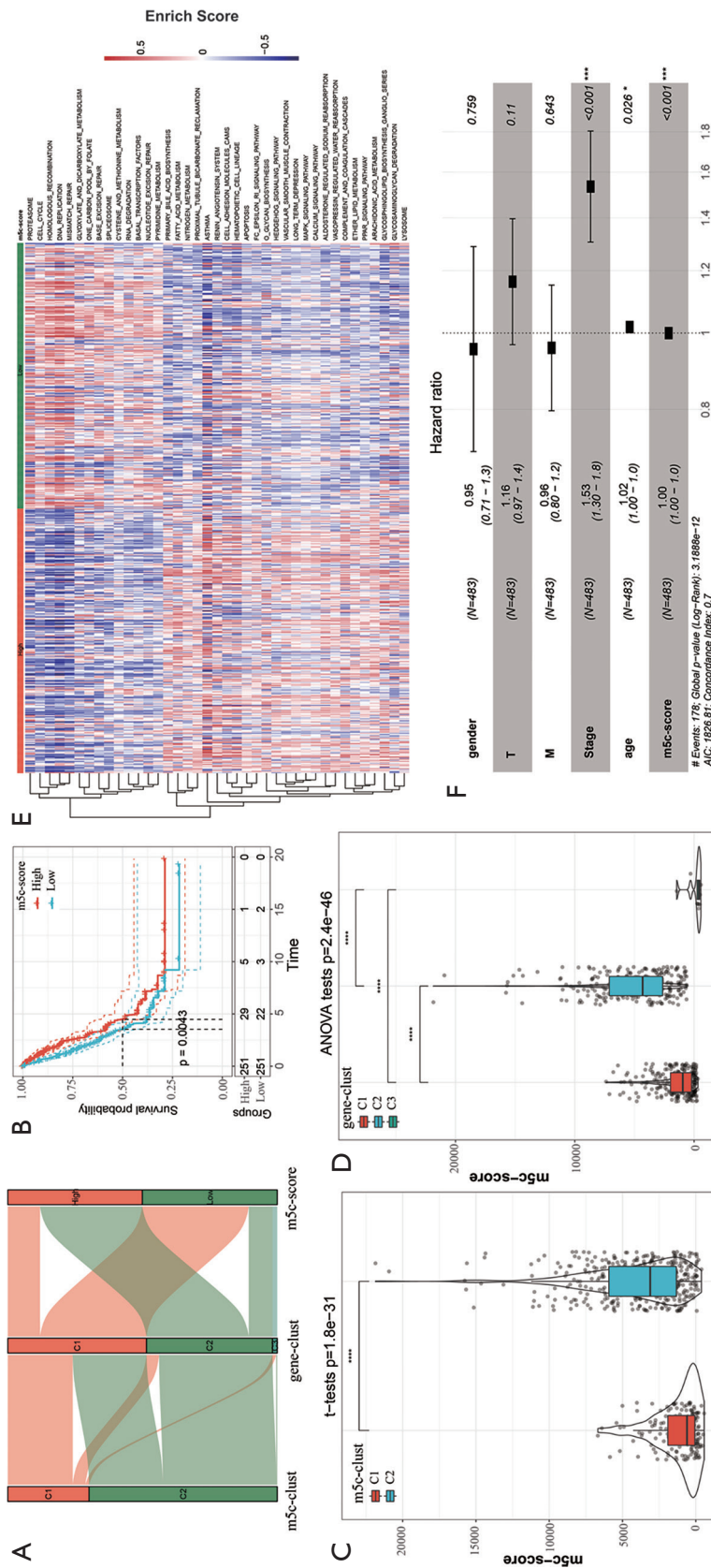


**Figure 9** Establishment of m<sup>5</sup>C-score model. (A) Alluvial diagram showing the changes of m<sup>5</sup>C clusters, gene clusters, and m<sup>5</sup>C scores; (B) survival analyses for both low and high m<sup>5</sup>C score patient groups; (C) distribution of patients with different m<sup>5</sup>C scores in three m<sup>5</sup>C gene clusters; (D) GSEA enrichment analysis showing the activation states of biological pathways in both high and low m<sup>5</sup>C score groups; (E) multivariate Cox regression analysis for m<sup>5</sup>C score in LUAD patients shown by forest plot. \*, P<0.05; \*\*\*, P<0.001; \*\*\*\*, P<0.0001. GSEA, gene set variation analysis; LUAD, lung adenocarcinoma.

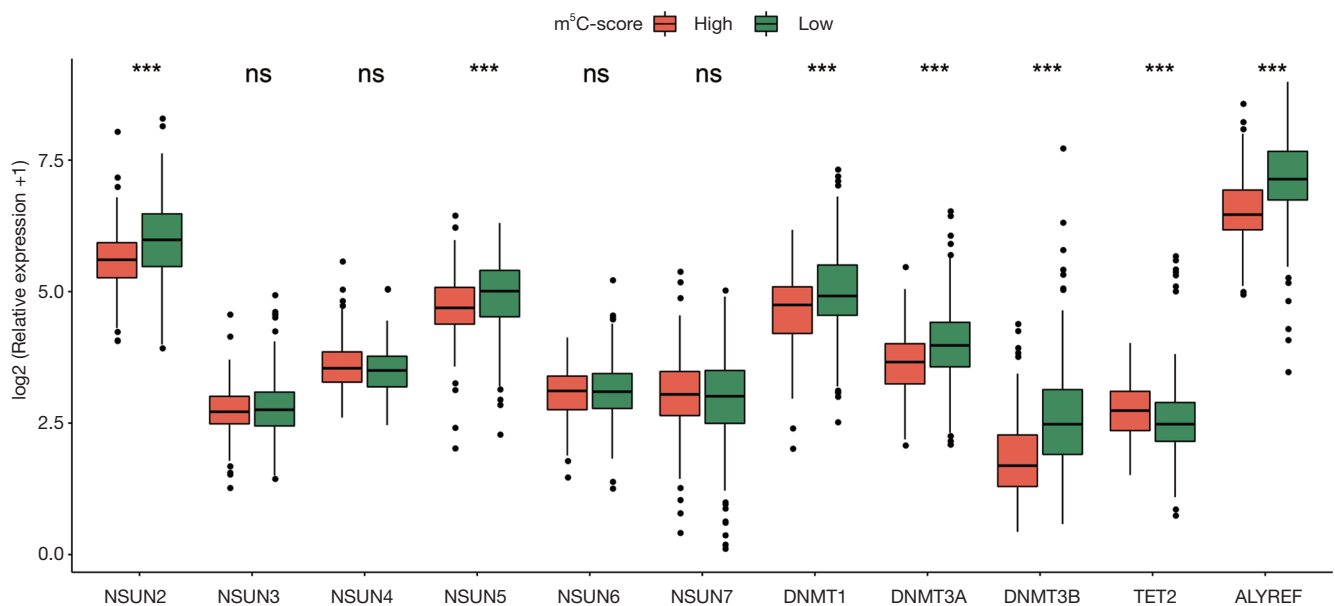


**Figure 10** The expression of 11  $m^5C$  regulators in both high and low  $m^5C$  score groups. ns, no significant difference; \*\*\*,  $P < 0.001$ .

scores. *Figure 11B* displays the prognosis of the high and low  $m^5C$  score groups; a high  $m^5C$  score may lead to a good prognosis, which was consistent with the results of TCGA.

#### GSVA analysis of the high and low $m^5C$ score groups

In order to further investigate mechanisms through which the  $m^5C$  score affected biological processes, we performed GSVA analysis using the R language. The results showed that the high  $m^5C$  score group was associated with immune pathways, such as the complement and coagulation cascades, leukocyte transendothelial migration, and the intestinal immune network for immunoglobulin A (IgA) production. Meanwhile, the low score group was associated with the pathways related to the stroma, such as basal resection and repair, cell cycle, etc. (*Figure 11C*).

These results verified that high  $m^5C$  scores were related to an immune desert type, which predicted a good prognosis, while low  $m^5C$  scores indicated an immune exclusion phenotype, which suggested a poor prognosis. The table online (<https://cdn.amegroups.com/static/public/tlcr-21-351-1.xlsx>) exhibits the enrichment scores of all samples in 186 pathways, and [Table S4](#) shows the enrichment results of the high and low  $m^5C$  score groups.

#### Composition of immune cells in the high and low levels of the $m^5C$ score model

To further verify the immunophenotype of the high and

low  $m^5C$  score groups of the dataset, we used CIBERSORT to analyze the composition of immune cells in the high and low  $m^5C$  score groups (*Figure 11D*). The high  $m^5C$  score exhibited more infiltration of resting CD4 memory T cells and resting mast cells, as well as less infiltration of M0 and M1 macrophages, which was similar to the immunocyte infiltration of gene cluster C2.

#### Discussion

With the development of deep sequencing and mass spectrometry (30), accumulating evidence has suggested that  $m^5C$  modification is very important for maintaining the normal physiological function of cells and organisms (31-36), while its abnormal distribution and expression are closely related to tumor development. Studies have confirmed that  $m^5C$  is involved in the progression of hepatocellular carcinoma (37,38). Also, there is increasing evidence that methylation regulatory factors can be used as prognostic and diagnostic markers of cancer (39-43). For example, the high expression of NSUN1 has been identified as a prognostic marker for non-small cell lung cancer (44-46). Recent studies have also confirmed that  $m^5C$  may affect the behavior of immune cells, such as  $CD^+$  T cells (47). Since most studies have focused on the effect of single TME cell types or regulators on tumor development, there remains a lack of comprehensive recognition of TME





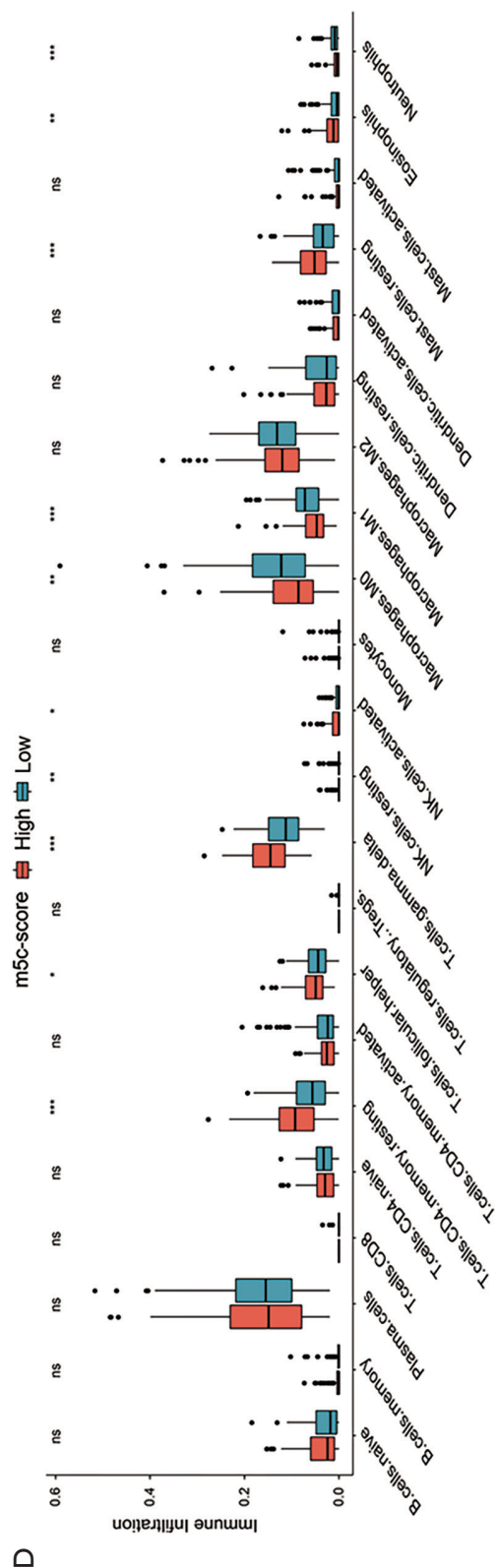


**Figure 11** GSVa analysis of the high and low m<sup>5</sup>C score groups. (A) The expression of 11 m<sup>5</sup>C regulators in both high and low m<sup>5</sup>C score groups in the GSE31210 dataset; (B) survival analysis of both high and low m<sup>5</sup>C score patient groups in the GSE31210 dataset; (C) GSVa enrichment analysis showing the activation states of biological pathways of both high and low m<sup>5</sup>C score groups in the GSE31210 dataset; (D) the abundance of each TME infiltration cell in both high and low m<sup>5</sup>C score groups in the GSE31210 dataset. ns, no significant difference; \*, P<0.05; \*\*, P<0.01; \*\*\*, P<0.001. GSVa, gene set variation analysis.

infiltration mediated by multiple m<sup>5</sup>C regulators. Further understanding of the role of different m<sup>5</sup>C modification patterns in the infiltration of TME cell will help to improve our understanding of the TME antitumor immune response and provide novel immunotherapy strategies.

In this study, two m<sup>5</sup>C methylation modification patterns were revealed according to 11 m<sup>5</sup>C regulators, which had remarkably distinct TME immune cell infiltration characterization. Also, three genomic subtypes of the m<sup>5</sup>C gene were identified based on 226 m<sup>5</sup>C phenotype-related DEGs, which were also significantly related to tumor occurrence. This further revealed the important role of m<sup>5</sup>C modification in influencing the TME landscape. Identification of the m<sup>5</sup>C modification patterns of individual tumors was crucial due to the individual heterogeneity of m<sup>5</sup>C modification. Thus, a scoring system was constructed to assess the m<sup>5</sup>C modification pattern of LUAD patients. The m<sup>5</sup>C cluster C2 exhibited a higher m<sup>5</sup>C score, and patients in the m<sup>5</sup>C cluster C2 showed better prognosis. The high m<sup>5</sup>C score group had a better prognosis, while the low m<sup>5</sup>C score group had a poor prognosis. These results were further verified in the GSE31210 dataset, which indicated that the m<sup>5</sup>C score was a reliable method for the integrated evaluation of distinct tumor m<sup>5</sup>C modification patterns. Comprehensive analyses also proved that the m<sup>5</sup>C score was an independent prognostic marker in LUAD. Functional enrichment analyses in the groups with better prognosis tended to be associated with immunity; m<sup>5</sup>C cluster C2 exhibited enrichment pathways related to immunity, such as the Fc epsilon RI signaling pathway, and the high m<sup>5</sup>C score group in the GSE31210 dataset was correlated with immune pathways, such as the complement and coagulation cascades, leukocyte trans-endothelial migration, and the intestinal immune network for IgA production. *NSUN2*, *NSUN5*, *DNMT1*, *DNMT3A*, *DNMT3B*, and *ALYREF* were highly expressed in m<sup>5</sup>C cluster C2, as well as in TCGA and GSE31210 low m<sup>5</sup>C score groups, which had a poor prognosis. Above, we analyzed immune cell infiltration, immune checkpoint characteristics, and functional enrichment analysis among different expression levels of DNMT3B in LUAD.

Our study provides some insight for clinical application. Our m<sup>5</sup>C score system could serve as a reliable and independent biomarker for predicting the prognosis of patients with LUAD. Our findings may help to screen suitable patients who can benefit from immune checkpoint inhibitor therapy. Further research based on these m<sup>5</sup>C regulators, which regulate TME immune

cell infiltration, may contribute to the discovery of novel immune drug combination treatment strategies or new immunotherapeutic agents, and promote the development of individual tumor immunotherapy.

The methylation modification patterns of gastric cancer, LUAD, and other cancers, which are mediated by the m<sup>6</sup>A modulator, and the invasion characteristics of the TME have been studied, and the m<sup>6</sup>A modulator is closely related to the tumor immunophenotype (48-53). Studies have also revealed that cross-talk between m<sup>6</sup>A and m<sup>5</sup>C regulators is associated with tumor immunogenicity and prognosis in 33 cancer types (54). In future studies, we will also aim to explore whether m<sup>5</sup>C and m<sup>6</sup>A have a synergistic effect on LUAD tumor microenvironmental characteristics and the patients' response to immunotherapy. We will also further investigate how genes (*NSUN2*, *NSUN5*, *DNMT1*, *DNMT3A*, *DNMT3B* and *ALYREF*) that are highly expressed in groups with poor prognosis work. In addition, we cannot rule out the possibility that m<sup>5</sup>C regulatory factors affect the behavior of the matrix in the TME. Some researchers have found that m<sup>5</sup>C is related to PM2.5-induced pulmonary fibrosis in mice (55), thus the regulatory behavior of m<sup>5</sup>C on the TME may be complex.

Our study had limitations that should be noted. Firstly, we did not consider the correlation between immune infiltration location and TME heterogeneity. Secondly, due to the limited clinical annotation in public datasets, the clinicopathological parameters detected in this study are not comprehensive, which may contribute to potential bias in the predictive performance when the m<sup>5</sup>C score signature served as a prognosis biomarker. Thirdly, due to the time constraints and lack of enough budget, we haven't carried out relevant experiments now. In future work, we will conduct further experiments to validate the results. Finally, due to the lack of overall clinical information in the datasets involved, we could not directly analyze the correlation between m<sup>5</sup>C score and the response of LUAD patients to immunotherapy.

## Conclusions

In this study, we found that m<sup>5</sup>C modification played a significant role in formation of TME diversity and complexity. Based on the characteristics of m<sup>5</sup>C modification, a score model was constructed to predict the prognosis of LUAD patients, which was also verified in the external dataset. We believe that m<sup>5</sup>C modification will have some implications for tumor immunotherapy in the future.

## Acknowledgments

This research was partly presented as an e-Poster at European Lung Cancer Virtual Congress during 25–27 March 2021.

*Funding:* This work was supported by the Chinese Society of Clinical Oncology/Beijing Xisike Clinical Oncology Research Foundation (Y-Young2020-0003) and the Shanghai Sailing Program (20YF1408300, 19YF1409200).

## Footnote

*Reporting Checklist:* The authors have completed the MDAR reporting checklist. Available at <http://dx.doi.org/10.21037/tlcr-21-351>

*Conflicts of Interest:* All authors have completed the ICMJE uniform disclosure form (available at <http://dx.doi.org/10.21037/tlcr-21-351>). The authors have no conflicts of interest to declare.

*Ethical Statement:* The authors are accountable for all aspects of the work in ensuring that questions related to the accuracy or integrity of any part of the work are appropriately investigated and resolved. The study was conducted in accordance with the Declaration of Helsinki (as revised in 2013).

*Open Access Statement:* This is an Open Access article distributed in accordance with the Creative Commons Attribution-NonCommercial-NoDerivs 4.0 International License (CC BY-NC-ND 4.0), which permits the non-commercial replication and distribution of the article with the strict proviso that no changes or edits are made and the original work is properly cited (including links to both the formal publication through the relevant DOI and the license). See: <https://creativecommons.org/licenses/by-nc-nd/4.0/>.

## References

1. Boccaletto P, Machnicka MA, Purta E, et al. MODOMICS: a database of RNA modification pathways. 2017 update. *Nucleic Acids Res* 2018;46:D303-D307.
2. Roundtree IA, Evans ME, Pan T, et al. Dynamic RNA Modifications in Gene Expression Regulation. *Cell* 2017;169:1187-200.
3. Chen K, Zhao BS, He C. Nucleic Acid Modifications in Regulation of Gene Expression. *Cell Chem Biol*

- 2016;23:74-85.
4. García-Vílchez R, Sevilla A, Blanco S. Post-transcriptional regulation by cytosine-5 methylation of RNA. *Biochim Biophys Acta Gene Regul Mech* 2019;1862:240-52.
  5. Squires JE, Patel HR, Nousch M, et al. Widespread occurrence of 5-methylcytosine in human coding and non-coding RNA. *Nucleic Acids Res* 2012;40:5023-33.
  6. Khoddami V, Cairns BR. Identification of direct targets and modified bases of RNA cytosine methyltransferases. *Nat Biotechnol* 2013;31:458-64.
  7. He X, Xu C. Immune checkpoint signaling and cancer immunotherapy. *Cell Res* 2020;30:660-9.
  8. Brahmer J, Reckamp KL, Baas P, et al. Nivolumab versus Docetaxel in Advanced Squamous-Cell Non-Small-Cell Lung Cancer. *N Engl J Med* 2015;373:123-35.
  9. Wu YL, Lu S, Cheng Y, et al. Nivolumab Versus Docetaxel in a Predominantly Chinese Patient Population With Previously Treated Advanced NSCLC: CheckMate 078 Randomized Phase III Clinical Trial. *J Thorac Oncol* 2019;14:867-75.
  10. Herbst RS, Baas P, Kim DW, et al. Pembrolizumab versus docetaxel for previously treated, PD-L1-positive, advanced non-small-cell lung cancer (KEYNOTE-010): a randomised controlled trial. *Lancet* 2016;387:1540-50.
  11. Borghaei H, Paz-Ares L, Horn L, et al. Nivolumab versus Docetaxel in Advanced Nonsquamous Non-Small-Cell Lung Cancer. *N Engl J Med* 2015;373:1627-39.
  12. Qureshi OS, Zheng Y, Nakamura K, et al. Trans-endocytosis of CD80 and CD86: a molecular basis for the cell-extrinsic function of CTLA-4. *Science* 2011;332:600-3.
  13. Sharpe AH, Pauken KE. The diverse functions of the PD1 inhibitory pathway. *Nat Rev Immunol* 2018;18:153-67.
  14. Champiat S, Derclé L, Ammari S, et al. Hyperprogressive Disease Is a New Pattern of Progression in Cancer Patients Treated by Anti-PD-1/PD-L1. *Clin Cancer Res* 2017;23:1920-8.
  15. van Kesteren MTR, Meeter M. How to optimize knowledge construction in the brain. *NPJ Sci Learn* 2020;5:5.
  16. Martini C, Marrucci W, Lucacchini A, et al. Specific inhibition of benzodiazepine receptor binding by some 1,2,3-triazole derivatives. *J Pharm Sci* 1988;77:977-80.
  17. Hanahan D, Weinberg RA. Hallmarks of cancer: the next generation. *Cell* 2011;144:646-74.
  18. Fridman WH, Pages F, Sautès-Fridman C, et al. The immune contexture in human tumours: impact on clinical outcome. *Nat Rev Cancer* 2012;12:298-306.
  19. Petitprez F, Meylan M, de Reynies A, et al. The Tumor Microenvironment in the Response to Immune Checkpoint Blockade Therapies. *Front Immunol* 2020;11:784.
  20. Fridman WH, Zitvogel L, Sautès-Fridman C, et al. The immune contexture in cancer prognosis and treatment. *Nat Rev Clin Oncol* 2017;14:717-34.
  21. Dunn GP, Old LJ, Schreiber RD. The three Es of cancer immunoediting. *Annu Rev Immunol* 2004;22:329-60.
  22. Gonçalves RC, Freire PP, Coletti D, et al. Tumor Microenvironment Autophagic Processes and Cachexia: The Missing Link? *Front Oncol* 2021;10:617109.
  23. Sacco A, Battaglia AM, Botta C, et al. Iron Metabolism in the Tumor Microenvironment-Implications for Anti-Cancer Immune Response. *Cells* 2021;10:303.
  24. Schoeler K, Aufschnaiter A, Messner S, et al. TET enzymes control antibody production and shape the mutational landscape in germinal centre B cells. *FEBS J* 2019;286:3566-81.
  25. Li H, Lu T, Sun W, et al. Ten-Eleven Translocation (TET) Enzymes Modulate the Activation of Dendritic Cells in Allergic Rhinitis. *Front Immunol* 2019;10:2271.
  26. Yue X, Lio CJ, Samaniego-Castruita D, et al. Loss of TET2 and TET3 in regulatory T cells unleashes effector function. *Nat Commun* 2019;10:2011.
  27. Chen X, Li A, Sun BF, et al. 5-methylcytosine promotes pathogenesis of bladder cancer through stabilizing mRNAs. *Nat Cell Biol* 2019;21:978-90.
  28. Janin M, Ortiz-Barahona V, de Moura MC, et al. Epigenetic loss of RNA-methyltransferase NSUN5 in glioma targets ribosomes to drive a stress adaptive translational program. *Acta Neuropathol* 2019;138:1053-74.
  29. Sato K, Tahata K, Akimoto K. Five Genes Associated With Survival in Patients With Lower-grade Gliomas Were Identified by Information-theoretical Analysis. *Anticancer Res* 2020;40:2777-85.
  30. Quinlan AR, Hall IM. BEDTools: a flexible suite of utilities for comparing genomic features. *Bioinformatics* 2010;26:841-2.
  31. Hänzelmann S, Castelo R, Guinney J. GSEA: gene set variation analysis for microarray and RNA-seq data. *BMC Bioinformatics* 2013;14:7.
  32. Newman AM, Liu CL, Green MR, et al. Robust enumeration of cell subsets from tissue expression profiles. *Nat Methods* 2015;12:453-7.
  33. Kanehisa M. Toward understanding the origin and evolution of cellular organisms. *Protein Sci* 2019;28:1947-51.
  34. Glasner H, Riml C, Micura R, et al. Label-free, direct localization and relative quantitation of the RNA

- nucleobase methylations m<sup>6</sup>A, m<sup>5</sup>C, m<sup>3</sup>U, and m<sup>5</sup>U by top-down mass spectrometry. *Nucleic Acids Res* 2017;45:8014-25.
35. Chen H, Yang H, Zhu X, et al. m(5)C modification of mRNA serves a DNA damage code to promote homologous recombination. *Nat Commun* 2020;11:2834.
  36. Trixl L, Lusser A. The dynamic RNA modification 5-methylcytosine and its emerging role as an epitranscriptomic mark. *Wiley Interdiscip Rev RNA* 2019;10:e1510.
  37. Sun Z, Xue S, Zhang M, et al. Aberrant NSUN2-mediated m(5)C modification of H19 lncRNA is associated with poor differentiation of hepatocellular carcinoma. *Oncogene* 2020;39:6906-19.
  38. Fish GD, Stanley JH, Miller KS, et al. Postbiopsy pneumothorax: estimating the risk by chest radiography and pulmonary function tests. *AJR Am J Roentgenol* 1988;150:71-4.
  39. Sun L, Liu WK, Du XW, et al. Large-scale transcriptome analysis identified RNA methylation regulators as novel prognostic signatures for lung adenocarcinoma. *Ann Transl Med* 2020;8:751.
  40. He Y, Yu X, Li J, et al. Role of m(5)C-related regulatory genes in the diagnosis and prognosis of hepatocellular carcinoma. *Am J Transl Res* 2020;12:912-22.
  41. Wang P, Wu M, Tu Z, et al. Identification of RNA: 5-Methylcytosine Methyltransferases-Related Signature for Predicting Prognosis in Glioma. *Front Oncol* 2020;10:1119.
  42. McHam ML, Fulton A. Albinism. *Int Ophthalmol Clin*. Winter 1992;32:185-200.
  43. Xue M, Shi Q, Zheng L, et al. Gene signatures of m<sup>5</sup>C regulators may predict prognoses of patients with head and neck squamous cell carcinoma. *Am J Transl Res* 2020;12:6841-52.
  44. Saijo Y, Sato G, Usui K, et al. Expression of nucleolar protein p120 predicts poor prognosis in patients with stage I lung adenocarcinoma. *Ann Oncol* 2001;12:1121-5.
  45. Sato G, Saijo Y, Uchiyama B, Kumano N, Sugawara S, Fujimura S, et al. Prognostic value of nucleolar protein p120 in patients with resected lung adenocarcinoma. *J Clin Oncol* 1999;17:2721-7.
  46. Uchiyama B, Saijo Y, Kumano N, et al. Expression of nucleolar protein p120 in human lung cancer: difference in histological types as a marker for proliferation. *Clin Cancer Res* 1997;3:1873-7.
  47. Guo G, Wang H, Shi X, Yet al. Disease Activity-Associated Alteration of mRNA m(5) C Methylation in CD4(+) T Cells of Systemic Lupus Erythematosus. *Front Cell Dev Biol* 2020;8:430.
  48. Zhang B, Wu Q, Li B, et al. m(6)A regulator-mediated methylation modification patterns and tumor microenvironment infiltration characterization in gastric cancer. *Mol Cancer* 2020;19:53.
  49. Li Y, Gu J, Xu F, et al. Molecular characterization, biological function, tumor microenvironment association and clinical significance of m6A regulators in lung adenocarcinoma. *Brief Bioinform* 2020. [Epub ahead of print]. doi: 10.1093/bib/bbaa225.
  50. Xu S, Tang L, Dai G, et al. Expression of m6A Regulators Correlated With Immune Microenvironment Predicts Therapeutic Efficacy and Prognosis in Gliomas. *Front Cell Dev Biol* 2020;8:594112.
  51. Xu F, Zhang Z, Yuan M, et al. M6A Regulatory Genes Play an Important Role in the Prognosis, Progression and Immune Microenvironment of Pancreatic Adenocarcinoma. *Cancer Invest* 2021;39:39-54.
  52. Lin S, Xu H, Zhang A, et al. Prognosis Analysis and Validation of m(6)A Signature and Tumor Immune Microenvironment in Glioma. *Front Oncol* 2020;10:541401.
  53. Fang J, Hu M, Sun Y, et al. Expression Profile Analysis of m6A RNA Methylation Regulators Indicates They Are Immune Signature Associated and Can Predict Survival in Kidney Renal Cell Carcinoma. *DNA Cell Biol* 2020. [Epub ahead of print]. doi: 10.1089/dna.2020.5767.
  54. Chen YT, Shen JY, Chen DP, et al. Identification of cross-talk between m(6)A and 5mC regulators associated with onco-immunogenic features and prognosis across 33 cancer types. *J Hematol Oncol* 2020;13:22.
  55. Han X, Liu H, Zhang Z, et al. Epitranscriptomic 5-Methylcytosine Profile in PM2.5-induced Mouse Pulmonary Fibrosis. *Genomics Proteomics Bioinformatics* 2020;18:41-51.

**Cite this article as:** Chen H, Ge XL, Zhang ZY, Liu M, Wu RY, Zhang XF, Xu LP, Cheng HY, Sun XC, Zhu HC. M<sup>5</sup>C regulator-mediated methylation modification patterns and tumor microenvironment infiltration characterization in lung adenocarcinoma. *Transl Lung Cancer Res* 2021;10(5):2172-2192. doi:10.21037/tlcr-21-351